Strong coupling between surface plasmon polariton and laser dye rhodamine 800

Cite as: Appl. Phys. Lett. **99**, 051110 (2011); https://doi.org/10.1063/1.3619845
Submitted: 21 April 2011 • Accepted: 08 July 2011 • Published Online: 03 August 2011

Federico Valmorra, Markus Bröll, Stephan Schwaiger, et al.

Strong coupling between surface plasmon polariton and laser dye rhodamine 800

Federico Valmorra, Markus Bröll, Stephan Schwaiger, Nadine Welzel, Detlef Heitmann, and Stefan Mendach[a)]

Institut für Angewandte Physik und Mikrostrukturforschungszentrum, Universität Hamburg, Jungiusstrasse 11, Hamburg D-20355, Germany

(Received 21 April 2011; accepted 8 July 2011; published online 3 August 2011)

We report on strong coupling between surface plasmon polaritons on a thin silver film and laser dye Rhodamine 800. Attenuated total reflection measurements reveal that the pure surface plasmon polaritons interact with the Rhodamine 800 absorption lines exhibiting pronounced anticrossings in the dispersion relation. We show that the corresponding energy gap can be tailored by the concentration of dye molecules in the dielectric matrix between 50 meV and 70 meV. We can well model our data by a classical transfer matrix approach as well as by a quantum mechanical coupled oscillator ansatz. © *2011 American Institute of Physics*. [doi:10.1063/1.3619845]

In recent years, the interaction of surface plasmon polaritons (SPPs)[1] with (organic) quantum emitters became a hot topic,[2–7] once again after the 70s,[8,9] due to the fast development of the field of nanophotonics.

In particular, the coupling between a SPP and an optically active medium, e.g., a dye, is a topic of interest, since it offers a wide spectrum of applications. One is the possibility to overcome SPPs losses with gain in the dielectric material.[10–15] Others are the use of coupling a SPP to an absorber to achieve an absorption-induced transparency,[16] or a possibility to slow down light.[17–19] In all these applications, the control of the coupling strength is an important task to achieve.

The objective of this letter is the study of the coupling of SPPs with the laser dye Rhodamine 800 (R800, produced by Sigma-Aldrich). The coupling results in an anticrossing of the SPP excitation and the dye absorption.[20] By performing reflection measurements, we investigate this anticrossing and, therefore, retrieve the coupling strength. In particular, we investigate the tuneability of this coupling by varying the dye concentration. Rhodamine 800, of the same class as the widely used Rhodamine6G, is important for devices working in the long wavelength part of the visible spectrum. We observe strong coupling between SPPs and Rhodamine 800 reflected in a pronounced anticrossing between the pure SPP dispersion relation and the Rhodamine 800 absorption line. We show that the corresponding energy gap can be tailored by the concentration of dye molecules between 50 meV and 70 meV.

The interaction of SPPs with R800 was studied by means of attenuated total reflection (ATR) at the planar interface between a layer of silver and a layer of Poly(methyl methacrylate) (PMMA) matrix containing the dye. The sample structure is sketched in Fig. 1(b). A 55 nm thick silver layer was thermally evaporated onto a glass substrate at room temperature and 10^{-8} mbar. On top of the silver layer, a PMMA-dye layer was spin-coated. The PMMA-dye layer solution used for the spin coating process was put together from a solution of R800, liquid PMMA, and thinner in the right proportions to get the desired layer thickness and dye concentration. Particularly for high dye concentrations, undesired clusters formed in the solution. A 200 nm filter was used for all PMMA-dye solutions to eliminate these clusters before spin coating and guarantee smooth PMMA-silver interfaces. The PMMA layer thickness was monitored by atomic force microscopy (AFM). The silver layer thickness was monitored *in situ* during thermal evaporation by a quartz oscillator.

In the following, we focus on three samples with similar silver thickness and similar PMMA thickness but varying dye concentration ($C_H > C_L$ and $C_0 = 0$). Due to the formation and filtering of clusters during the preparation process, the exact values for the final dye concentrations in the PMMA films are unknown. The dye concentration in the liquid PMMA before filtering and spin coating was 30 g/l and 5 g/l for sample C_H and sample C_L, respectively.

Figure 1(a) sketches the ATR setup. The reflection is measured in Kretschmann-Raether configuration[1,21] with the glass substrate of the sample (with refractive index about $n_{sub} = 1.52$ in the energy range of interest) in contact with a Schott k-n5-glass prism ($n_{prism} = 1.52$) via immersion oil ($n_{oil} = 1.52$). The p-polarized light is measured for varying wavelength and angle of incidence θ after attenuated total internal reflection at the glass-metal interface. A drop in the reflected intensity appears if a surface plasmon is excited at the silver PMMA interface.

The orange solid line in Fig. 2(b) shows the absorption spectrum $A = 1 - T - R$ of the Rhodamine 800 dye in a PMMA matrix measured in perpendicular transmission on a reference sample. The absorption maxima at $\lambda_1 = 626$ nm ($E_1 = 1.98$ eV) and $\lambda_2 = 686$ nm ($E_2 = 1.81$ eV) are depicted by vertical dashed orange lines. The thick blue lines in Fig. 2(a) represent ATR spectra of sample C_H, which has the highest dye

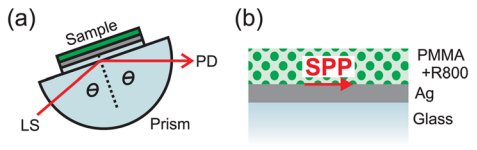

FIG. 1. (Color online) (a) Sketch of the attenuated total reflection setup, LS: tunable light source (Koheras), PD: Photo diode (b) sample structure: glass substrate (light blue), silver layer (gray), PMMA layer (dotted green) doped with different concentrations of Rhodamine800.

[a)]Author to whom correspondence should be addressed. Electronic mail: smendach@physnet.uni-hamburg.de.

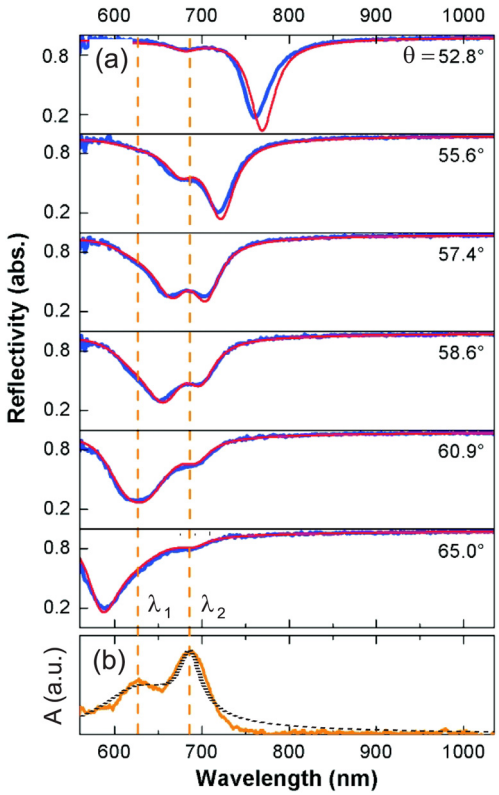

FIG. 2. (Color online) (a) Reflectivity signal measured vs wavelength (blue thick line) at different angles of incidence for sample C_H. The curves resulting from the analytical transfer matrix method model described in the text (red thin line) have been superimposed for comparison. (b) R800 absorption spectrum (orange solid line). To better visualize the SPP-dye interaction, the absorption peaks position has been marked (vertical orange dashed lines). The black dotted line plots the imaginary part of two Lorentzians with parameters retrieved from transfer matrix fits of sample C_H (cf., Table I). Both curves are normalized to their maximum value.

concentration, measured at different angles of incidence θ. Two clear anticrossings are observed in correspondence to the R800 absorption peaks at λ_1 and λ_2. Increasing the angle θ, with the SPP dip moving towards the absorption region, in correspondence to the nearest absorption peak at λ_2, a second dip develops and deepens at expenses of the first one. At 57.4°, the two reflectivity minima have equal depth. As the angle θ is further increased, this second dip further deepens and moves towards shorter wavelength, whereas the first dip becomes more shallow and its minimum asymptotically tends to the absorption peak wavelength. The very same behavior is also observed in correspondence to the absorption peak at λ_1, with an initially shallow additional dip already present at 55.6°. This additional minimum has the same depth as the second one at 60.9°, but they are not clearly resolved. The described anticrossing behavior can be observed more directly when plotting the reflection minima frequencies over the wave vector k_x, i.e., the experimentally observed dispersion, as shown in Figs. 3(a) and 3(b) for sample C_H and sample C_L, respectively. The minima positions were obtained from the reflection curves by Lorentz fits. For both samples, we observe anticrossing behavior indicating strong coupling between SPP and R800 dye.

In the following, we analyze the experimental data in more detail by means of classical transfer matrix method (TMM) calculations as well as by a quantum mechanical coupled oscillator ansatz (QMO).

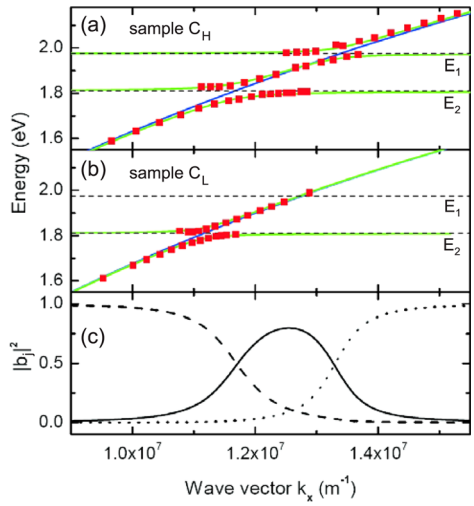

FIG. 3. (Color online) (a) and (b) (Red dots) Dispersion relations for sample C_H and sample C_L retrieved from the multiple minima in the spectra reflectivity vs wavelength. (Blue line) Calculated dispersion relation for the same sample without dye in the PMMA layer. (Green lines) Coupled oscillators fit for the dye-SPP interaction. (c) Mixing coefficients for the middle branch between E_1 and E_2 retrieved from the coupled-oscillators fit on sample C_H. Solid line: B_1 , dotted line: B_2 , dashed line: B_3.

Analytical fits of the ATR measurements based on classical TMM calculations[22] are shown as red curves in Fig. 2(a). We modeled the system as a multilayer composed of half infinite space of glass, a layer of silver, a layer of R800-PMMA, and half infinite space of air. The permittivity function of the Schott k-n5-glass was taken from the supplier specifications. The permittivity of silver was derived from the fit of ATR measurements on a reference sample without PMMA layer. The permittivity of PMMA was correspondingly retrieved from sample C_0 which contains no dye. The contribution of the R800 in the PMMA was included by adding two Lorentzians with transition energies $E_1 = \hbar\omega_{0,1} = 1.98$ eV ($\lambda_1 = 626$ nm) and $E_2 = \hbar\omega_{0,2} = 1.81$ eV ($\lambda_2 = 686$ nm), taken from the absorption spectrum of Fig. 2(b), to the fitted PMMA permittivity:

$$\epsilon_{Diel}(\omega) = \epsilon_{PMMA}(\omega) + \sum_{j=1}^{2} \frac{f_j \omega_{0,j}^2}{\omega_{0,j}^2 - \omega^2 - i\gamma_j \omega}, \qquad (1)$$

with ϵ_{PMMA} permittivity of the PMMA matrix, f oscillator strength of the transition, and $\hbar\gamma$ width of the transition. The sum is carried over the two peaks in the R800 absorption spectrum indicated with index '1' and '2' in Eq. (1).

The parameters retrieved with the TMM model for the R800-Lorentzians are displayed in Table I together with the retrieved layer thicknesses, which are consistent within 10% with AFM and quartz oscillator measurements. As exemplified with sample C_H by the black dotted curve in Fig. 2(b), the imaginary parts of the retrieved R800-Lorentzians show a good qualitative agreement with the dye absorption in the reference sample. In agreement with a higher dye concentration in sample C_H, the oscillator strengths f_1 and f_2 of sample C_H are larger than those of sample C_L by a factor of 1.3 and 1.6, respectively. The difference in the increase factors for f_1 and f_2 occurs because the ratio of monomers and dimers, which contribute differently to f_1 and f_2, in general changes if the overall dye concentration is increased.[23]

TABLE I. Sample parameters retrieved from experimental data with the TMM model and the QMO model.

	Sample C_H	Sample C_L	Sample C_0	Model
t_{Ag}	54 nm	54 nm	40 nm	TMM
t_{PMMA}	69 nm	58 nm	72 nm	TMM
f_1	14×10^{-3}	11×10^{-3}	0	TMM
f_2	5.5×10^{-3}	3.4×10^{-3}	0	TMM
$\hbar\gamma_1$	0.35 eV	0.36 eV	0 eV	TMM
$\hbar\gamma_2$	0.10 eV	0.08 eV	0 eV	TMM
Δ_1	$\Delta_{1H} = 48$ meV	$\Delta_{1L} = 0$ meV	$\Delta_{10} = 0$ meV	QMO
Δ_2	$\Delta_{2H} = 70$ meV	$\Delta_{2L} = 49$ meV	$\Delta_{20} = 0$ meV	QMO

While all our data can be well reproduced by the classical transfer matrix calculations as shown in Fig. 2 and discussed above, we can also employ a quantum mechanical coupled oscillator model to fit the dispersion curve in Fig. 3 in terms of a strong coupling phenomenon. The possibility of discussing anticrossings of a quantum object dispersion and a cavity dispersion both classically or quantum mechanically has been pointed out by various publications, e.g., Ref. 24. The quantum mechanical coupled oscillator ansatz is described in detail, e.g., in Ref. 25 and was also used in Refs. 2, 4–6

$$\begin{pmatrix} E_{SPP}(k_x) & \Delta_1/2 & \Delta_2/2 \\ \Delta_1/2 & E_{1,dye} & 0 \\ \Delta_2/2 & 0 & E_{2,dye} \end{pmatrix} \begin{pmatrix} b_1 \\ b_2 \\ b_3 \end{pmatrix} = E(k_x) \begin{pmatrix} b_1 \\ b_2 \\ b_3 \end{pmatrix}, \quad (2)$$

where $E_{SPP}(k_x)$ is the SPP dispersion relation without dye, $E_{j,dye}$ are the dispersionless dye absorption energies related to peaks 'j', Δ_j are the coupling energies of the 'jth' absorption line and $E(k_x)$ is the resulting dispersion relation. The mixed state vector is related to the unperturbed ones via the coefficient vector as $|\Psi\rangle = b_1|\phi_{SPP}\rangle + b_2|\phi_{1,dye}\rangle + b_3|\phi_{2,dye}\rangle$

In Fig. 3, we present the SPP dispersion relation $E_{SPP}(kx)$ (solid blue lines), the absorption energies of the dye E_i (dashed black lines), and the coupled dispersion relation braches (green solid lines) which were derived as eigenvalues of the matrix in Eq. (2). As fitting parameters, the amplitudes of the energy splittings at E_1 and E_2 are found (cf., Table I). The energy splitting at E_2 is $\Delta_{2L} = 49$ meV for sample C_L and increases to $\Delta_{2H} = 70$ meV for sample C_H with higher dye concentration, where the ratio $\Delta_{2H}/\Delta_{2L} = 1.4$ is in the order of the oscillator strength increase factors discussed above. In contrast to Δ_2, where the oscillator strength is $\hbar\gamma_2 \approx 100$ meV, the energy splitting Δ_1 at E_1 is dominated by the much stronger oscillator damping $\hbar\gamma_1 \approx 350$ meV. In corresponding TMM calculations, we found that the energy splitting in our samples starts to decrease due to broadening for oscillator damping values above 100 meV. Due to this broadening, no energy splitting is resolvable with our fitting procedure for sample C_L at E_1, i.e., $\Delta_{1L} = 0$ meV. For sample C_H, we obtain $\Delta_{1H} = 48$ meV at E_1. In both samples, the energy splitting observed at E_1 is, therefore, smaller than the energy splitting observed at E_2, in spite of the fact that the oscillator strength f_1 is larger than f_2.

Determining the eigenvectors of the matrix in Eq. (2), i.e., the formulae for the coefficient vector, the single oscillator contributions to the different coupled dispersion relation branches can be derived. The squared moduli of the mixing coefficients b_i for the middle branch between E_1 and E_2 in Fig. 3(a) are plotted in Fig. 3(c) where the solid line indicates the pure SPP mixing coefficient whereas the dotted and dashed lines indicate the dye absorption line 1 and 2, respectively. It can be seen that the middle branch exhibits significant mixing of the pure SPP with both absorptions lines.

In conclusion, we measured the interaction of SPPs on a silver film with the laser dye R800 molecules in a PMMA matrix. By means of ATR spectroscopy, we observe a pronounced anticrossing in the respective dispersions. Our data can be fitted both, with a classical transfer matrix model or with a quantum mechanical coupled oscillator model. From the latter, we extract energy splittings of up to 70 meV and mixing of the surface plasmon with both R800 absorption lines resulting in a hybridized excitation. Furthermore, we show that the energy splitting can be tuned by the concentration of dye R800 molecules in the PMMA matrix. This controlled coupling of surface plasmons and dye molecules allows to tailor the hybridized excitation and its dispersion relation with a possible application, e.g., as a slow light material[16] or an absorption induced transparent material with a tunable transmission.[17–19]

We gratefully acknowledge Wolfgang Hansen for fruitfull discussions and financial support of the Deutsche Forschungsgemeinschaft via the GrK 1286 and the city of Hamburg via LExI 'Nanospintronics.'

[1]H. Raether, *Surface Plasmons on Smooth and Rough Surfaces and on Gratings* (Springer, Berlin, 1988).
[2]J. Bellessa, C. Bonnand, J. Plenet, and J. Mugnier, Phys. Rev. Lett. **93**, 036404 (2004).
[3]C. Bonnand, J. Bellessa, and J. C. Plenet, Phys. Rev. B **73**, 245330 (2006).
[4]D. E. Gómez, K. C. Vernon, P. Mulvaney, and T. J. Davis, Appl. Phys. Lett. **96**, 073108 (2010).
[5]D. E. Gómez, K. C. Vernon, P. Mulvaney, and T. J. Davis, Nano Lett. **10**, 274 (2010).
[6]T. K. Hakala, J. J. Toppari, A. Kuzyk, M. Pettersson, H. Tikkanen, H. Kunttu, and P. Törmä, Phys. Rev. Lett. **103**, 053602 (2009).
[7]C. Symonds, C. Bonnand, J. C. Plenet, A. Brehier, R. Parashkov, J. Lauret, E. Dleporte, and J. Bellessa, New J. Phys. **10**, 065017 (2008).
[8]A. Brillante and I. Pockrand, J. Mol. Struct. **79**, 169 (1982).
[9]I. Pockrand, J. D. Swalen, R. Santo, A. Brillante, and M. Philipott, J. Chem. Phys. **69**, 4001 (1978).
[10]S. Wuestner, A. Pusch, K. L. Tsakmakidis, J. M. Hamm, and O. Hess, Phys. Rev. Lett. **105**, 127401 (2010).
[11]S. Xiao, V. P. Drachev, A. V. Kildishev, X. Ni, U. K. Chettiar, H.-K. Yuan, and V. M. Shalaev, Nature **466**, 735 (2010).
[12]J. Seidel, S. Grafström, and L. Eng, Phys. Rev. Lett. **94**, 177401 (2005).
[13]M. A. Noginov, G. Zhu, M. Mayy, B. Ritzo, N. Noginova, and V. Podolskiy, Phys. Rev. Lett. **101**, 226806 (2008).
[14]I. D. Leon and P. Berini, Nature Photon. **4**, 382 (2010).
[15]A. Rottler, M. Broell, S. Schwaiger, D. Heitmann, and S. Mendach, Opt. Lett. **36**, 1240 (2011).
[16]J. A. Hutchison, D. M. O'Carroll, T. Schwartz, C. Genet, and T. W. Ebbesen, *Angew. Chem., Int. Ed.* **50**, 2085 (2011).
[17]L. V. Hau, S. E. Harris, Z. Dutton, and C. H. Behroozi, Nature **397**, 594 (1999).
[18]S. Zhang, D. A. Genov, Y. Wang, M. Liu, and X. Zhang, Phys. Rev. Lett. **101**, 047401 (2008).
[19]C. Wu, A. B. Khanikaev, and G. Shvets, Phys. Rev. Lett. **106**, 107403 (2011).
[20]I. Pockrand and J. D. Swalen, J. Opt. Soc. Am. **68**, 1147 (1978).
[21]E. Kretschmann and H. Raether, Zeitschrift für Naturforschung A **23**, 2135 (1968).
[22]M. Born and E. Wolf, *Principles of Optics* (Cambridge University Press, Cambridge, 1997).
[23]K. Sekiguchi, S. Yamaguchi, and T. Tahara, J. Phys. Chem. A **110**, 2601 (2006).
[24]Y. Zhu, D. J. Gauthier, S. Morin, Q. Wu, H. Carmichael, and T. Mossberg, Phys. Rev. Lett. **64**, 2499 (1990).
[25]A. Armitage, M. Skolnick, A. Kavokin, D. Whittaker, V. Astratov, G. Gehring, and J. Roberts, Phys. Rev. B **58**, 15367 (1998).